Advanced material model for numerical simulations of fine blanking

JÁNSKÁ Danuše[1,a], URBÁNEK Miroslav[1,b] and MAŠEK Martin[1,c]

[1]COMTES FHT, Metals Research Institute; Průmyslová 995, 334 41 Dobřany, Czech Republic

[a]danuse.janska@comtesfht.cz, [b]miroslav.urbanek@comtesfht.cz, [c]martin.masek@comtesfht.cz

Keywords: fine blanking, 1.4301 steel, FEM, material model

Abstract. Advanced manufacturing processes, including fine blanking, are widely used in the mass production of sheet metal parts. In the present article, numerical modelling and a real-world test of fine blanking are discussed with a focus on material characterization. The material was 1.4301 stainless steel and its model was constructed using measured mechanical properties. Tensile tests, plane strain tests and shear tests were carried out to determine steel characteristics under various stress states. All the tests were performed at room temperature and under quasi-static conditions. Local strains were determined using the ARAMIS digital image correlation (DIC) system from GOM company. After testing, metallographic analysis of the specimens was conducted for characterizing their fracture surfaces. By correlating the data from the DIC system, results of numerical modelling and metallographic examination, the instant of failure initiation in a specimen can be determined. When a ductile failure model is calibrated against tests under various stress states and used for modelling of blanking, it improves the description and the accuracy of the computational model of the process. The choice of the failure model has a substantial impact on the calculated magnitude of fine blanking force. To validate the material models chosen, an additional fine blanking test and metallographic examination were performed in order to assess the creation and shape of the sheared edge. A material model developed and validated by this procedure becomes useful in the design and optimization of real-world blanking processes.

Introduction

Fine blanking is a rapid and effective material parting method, which is employed in the series production of sheet parts. In fine blanking, a punch exerts a shearing action, whereby a blank is separated from a sheet or sheet strip by shear deformation. Given today's increasing demands on the quality and lifetime of engineering parts, it becomes necessary to focus on the blanking process and on the effects of its key aspects, such as the clearance between the die and the punch, their geometries, the punch speed and the hold-down force, on sheared edge quality. Burrs and distortions, which may occur on the sheared edge, require additional finishing operations, such as grinding, and therefore longer production times and higher costs.

Blanking is most often studied experimentally, which is an expensive undertaking, the results of which are generally impossible to apply to other parts with different shapes. For these reasons, finite element (FE) calculations are very useful because their predictions enable engineers to reduce the number of actual tests needed. Using computational methods, one can predict the shape and quality of the sheared edge, the strains, residual stresses and failure and distortion in the sheet stock and the product.

This paper explores the process of fine blanking from a 2 mm sheet of ordinary chromium-nickel austenitic stainless steel 1.4301.

Fine Blanking

Fine blanking (Fig. 1) is a shearing process which has been enhanced to produce blanks of high precision and surface quality which can be used directly for assembly of products. The clearance between the punch and the die is of major importance. Whereas the clearance per side in conventional shearing is normally 3–10% of the sheet thickness, the clearance in fine blanking is 0.5% of the thickness of the work material. In the experiment reported here, the clearance was 0.03 mm per side. The smaller is the clearance, the closer is the stress state to pure shear and the smaller are the undesirable tensile stress components under the bending load. The sheared edge radius is 0.2 mm. Experimental validation of the material models was performed with the use of a test tool which conformed to the above-detailed requirements for precision. The test tool had been developed for servo-electric test machine Zwick 250 (Fig. 2).

Fs – blanking force
Fr – impingement ring force
Fg – counterpunch holding force
 s – thickness of the work material
Sp – die clearance
1 – die
2 – impingement ring
3 – punch
4 – counterpunch-ejector
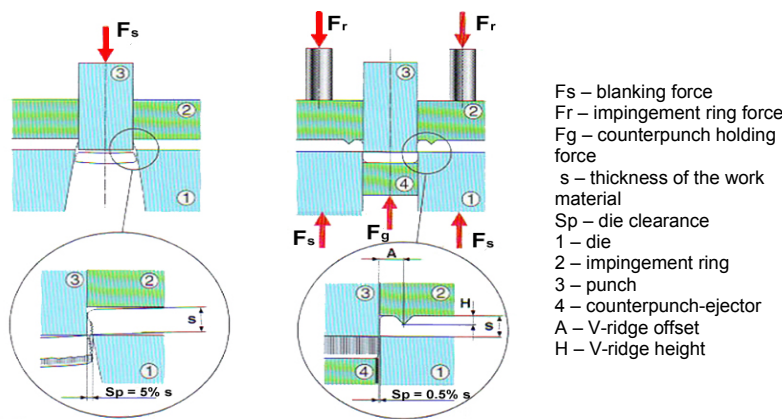A – V-ridge offset
H – V-ridge height

Fig. 1 Illustration of differences between conventional punching and fine blanking

Fig. 2: Experimental test set-up in ZWICK machine

Material models

Considering the toughness of stainless steel, an appropriate material model should be chosen for numerical modelling of its behaviour. In this work, uncoupled models were used, in which plasticity and damage are accounted for independently.

Plasticity

When it comes to characterizing plasticity of material, the most-widely used formula is the Johnson-Cook (J-C) plasticity model (1). It is implemented in most commercial simulation codes. Many publications were devoted to its calibration, [8] . Its equation includes the following material constants: A – yield strength; B and n – material constants which characterize the real-world stress-strain curve. Together, these constants characterize the work-hardening curve under quasi-static conditions.

$$\sigma_y = \left(A + B\bar{\varepsilon}^{p^n}\right) \tag{1}$$

Fracture

In this work, four different fracture models were considered. Depending on formulation, each of them requires a different number of mechanical tests for calibration. Ductile fracture is a process which leads to macroscopic separation in material. It is understood as a sequence of formation, growth and coalescence of voids which are present in the material. In continuum mechanics, it is described through stress state-related quantities. These quantities include

triaxiality, a characteristic of three-dimensionality of the stress state, and the Lode parameter (2) which accounts for the effects of shear stress state.

$$\bar{\theta} = 1 - \left(\frac{6\theta}{\pi}\right) = 1 - \frac{2}{\pi}\arccos\xi \qquad\qquad \xi = \left(\frac{r}{q}\right)^3 = \cos(3\theta) \qquad\qquad (2)$$

Below, the individual fracture models are described, including the minimum number of mechanical tests required for their calibration.

Johnson-Cook model

This model characterizes fracture behaviour of material under various stress states. Equation (3) includes material constants D_1, D_2 and D_3, which characterize the fracture curve for various stress triaxiality values under quasi-static conditions. Triaxiality values vary with the stress state. Generally, they are in the range from -1 to 1.

$$\varepsilon_{f\ JC} = \left(D_1 + D_2 e^{D_3\sigma^*}\right)[1 + D_4 * \ln\dot{\varepsilon}^*][1 + D_5 T^*] \qquad\qquad (3)$$

Bao-Wierzbicki model

The second model was the Bao-Wierzbicky (B-W) fracture model. It is calibrated against tensile test data. Bao-Wierzbicky ductile fracture model comprises three regions which differ according to stress state. Region I ($1/3 < \eta$) involves high triaxiality values. Stress triaxiality induces formation, growth and coalescence of voids, a failure mechanism which occurs in tension. In region II ($0 < \eta < 1/3$) triaxiality values are positive but low, which is reflected in combined failure modes.
Region III ($-1/3 < \eta \leq 0$) comprises negative stress triaxiality values, at which shear failure occurs.
The failure initiation locus for the Bao-Wierzbicki model is defined in terms of equations (4).

Region I	Region II	Region III	
$\bar{\varepsilon}_{f\ BWI} = a\dfrac{\eta_0}{\eta}$	$\bar{\varepsilon}_{f\ BWII} = b + (a-b)\left(\dfrac{\eta}{\eta_0}\right)^2$	$\bar{\varepsilon}_{f\ BWIII} = \dfrac{a}{1+3\eta}$	(4)

Constant a is the plastic strain at fracture in pure shear ($\eta = 0$). Constant b is the plastic strain at fracture in uniaxial tension ($\eta = 1/3$). Parameter b can be derived from tensile test data using formula (5), where A_0 denotes the cross-sectional area before the test and A_f is the fracture surface area. Constant a is calculated using equation (6).

$$b = \ln\left(\frac{A_0}{A_f}\right) \qquad (5) \qquad\qquad a = b\left(\frac{\sqrt{3}}{2}\right)^{\frac{1}{n}} \qquad (6)$$

MAX shear model

The MAX shear model is calibrated against data from shear test specimens. The maximum shear stress criterion, known as the Tresca criterion, postulates that failure occurs when the largest shear stress reaches critical value $\tau_{max} = C_1$.

Hosford-Coulomb model

Hosford-Coulomb (H-C) model is an expansion of the classical Mohr-Coulomb criterion. The H-C model was proposed by Bai-Wierzbicky and presented by Mohr (Mohr and Marcadet, 2015). In this model, the Tresca stress has been replaced with Hosford equivalent stress (9) σ_{HF}. When this model is mapped to the triaxiality-Lode parameter space, a relationship is obtained, which was derived in [14] (10). The letters f denote Lode parameter-dependent functions. Values a, b and c must be determined by experiment.

$$\sigma_{HF} + C(\sigma_I + \sigma_{II}) = b \qquad (9)$$

$$\bar{\varepsilon}_{f\,HC}[\eta, \bar{\theta}] = b(1+c)^{\frac{1}{n}} \left(\left\{ \frac{1}{2} (f_1 - f_2)^a + (f_2 - f_3)^a + (f_1 - f_3)^a \right\}^{\frac{1}{a}} + c(2\eta + f_1 + f_3) \right)^{-\frac{1}{n}} \qquad (10)$$

In order to validate the above-described plasticity and fracture models, an experimental programme was developed and carried out. The experimental material was a cold-rolled sheet of 1.4301 stainless steel 2 mm in thickness.

Experimental programme

The purpose of the programme was to characterize stainless steel by determining its yield strength, ultimate strength, elongation, reduction of area and the force-displacement curve measured by means of an extensometer. The force-displacement data were input into the material models. Material constants were determined on the basis of and calibrated against mechanical test data for specimens shown in Fig. 3. The values obtained from this set of tests were used for characterizing the material in various stress states by means of the models of material behaviour under load: Johnson-Cook, Bao-Wierzbicky, Max shear and Hosford-Coulomb. The mechanical tests are described in detail below.

a) Specimen for tensile test

b) Specimen for tensile test with a hole

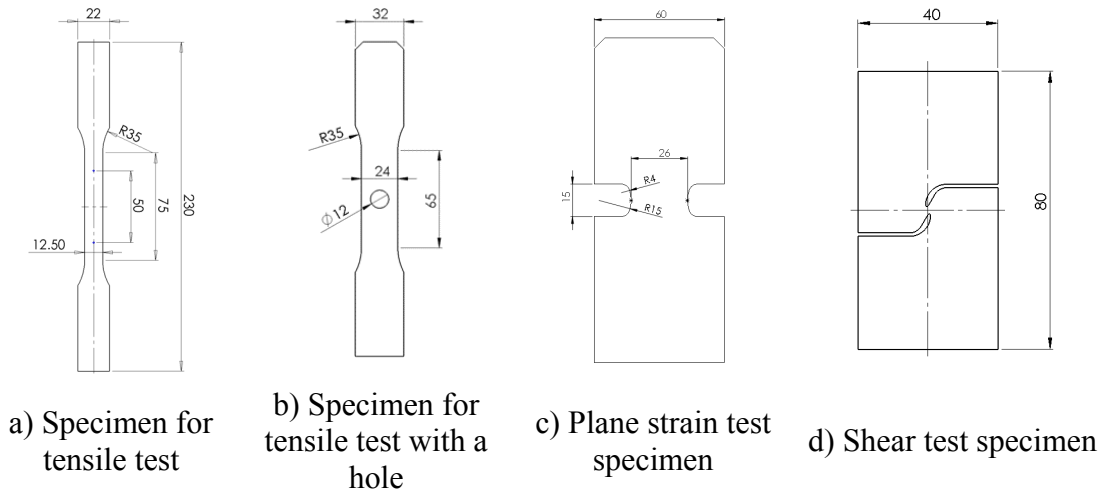c) Plane strain test specimen

d) Shear test specimen

Fig. 3: Geometries of test specimens

Tensile test data were used for characterizing the plastic behaviour of the material. The data from the other tests provided description of fracture in the material. All the tests were conducted under quasi-static conditions and at room temperature. Three test specimens were used for each of them to ensure that the results are statistically relevant. Local strains were evaluated using an ARAMIS DIC system with 12-MPix cameras (Fig. 4, Fig. 5, Fig. 6, Fig. 7)
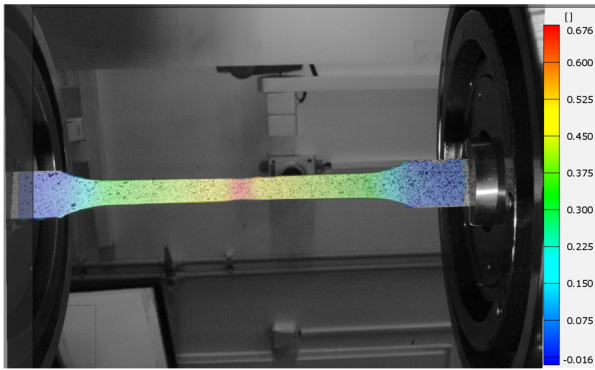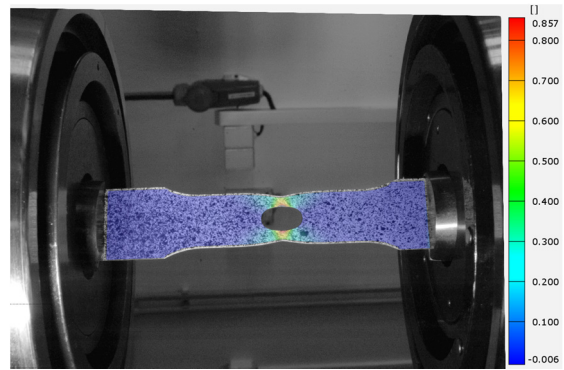
Fig. 4: Tensile test set-up

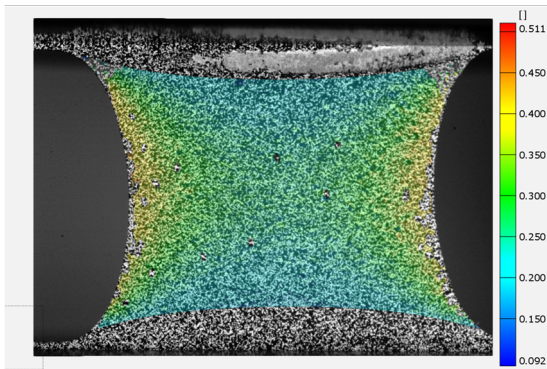Fig. 5: Test set-up for the specimen with a hole
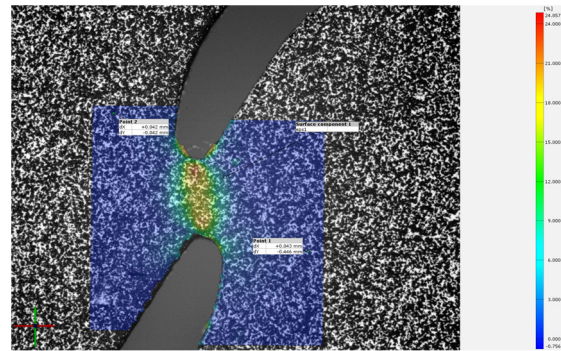

Fig. 6: Plane strain test specimen

Fig. 7: Shear test specimen

Calibration of material models

The material model which comprised the Johnson-Cook plasticity model was developed with the use of an optimization script. Using the script, material constants A, B and n were determined from the data for unnotched solid test specimens. The values of the constants were refined with the aid of numerical modelling to ensure they lead to an agreement between the simulation model and the real-world test data (Fig. 8). The criterion was the match between the force-displacement plots. The simulation-based refinement of plasticity characteristics did not take into account damage.
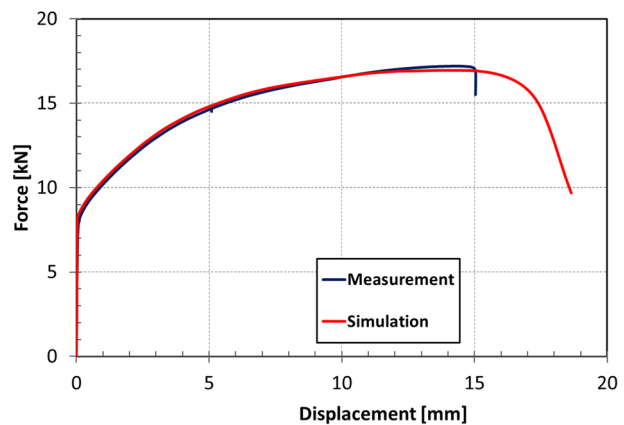

Fig. 8 Diagram of tensile tests and comparison with numerical simulation

Fracture behaviour was simulated by successively applying the Johnson-Cook fracture, Bao-Wierzbicky, MAX shear, and Hosford-Coulomb models. Based on triaxiality and fracture strain values found from mechanical tests and calculations, threshold values were determined and the curves for individual models were fitted to them. The material constants for the Johnson

Cook plasticity and Johnson Cook fracture models and the Hosford-Coulomb model were calibrated using an optimization script. They are given in Table 1.

Table 1: Calibrated simulation parameters

Johnson-Cook plasticity	A	B	n	
	190	1210	0.48	
Johnson-Cook fracture	D1	D2	D3	
	-0.45	1.8	-0.6	
Bao-Wierzbicky fracture	b	n		
	0.67	0.48		
MAX shear fracture	C	n		
	5.5	0.48		
Hosford-Coulomb fracture	a	b	c	n
	0.9908	1.1748	0.2	0.2743

For illustration, the graphs below show the comparison between mechanical test diagrams and curves from numerical modelling using Bao-Wierzbicky model. The diagram from tensile tests on specimens with a hole is shown in Fig. 9. The plane strain test diagram and evaluation are presented in Fig. 10. The shear test is evaluated in Fig. 12.
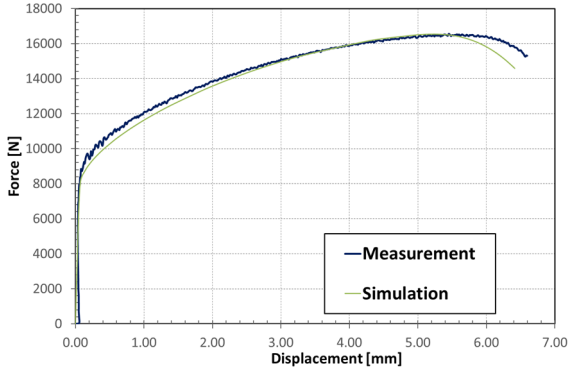

Fig. 9 Tensile test diagram for specimens with a hole and a numerical model curve
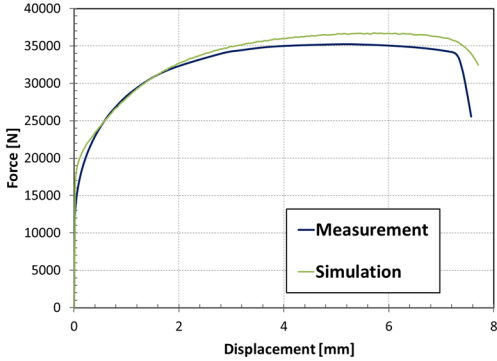

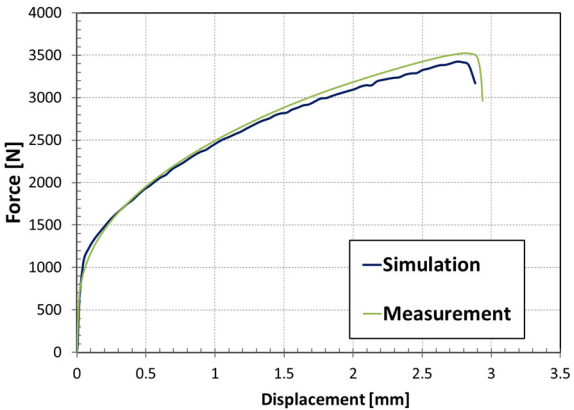Fig. 10 Diagram of plane strain tests and comparison with numerical simulation

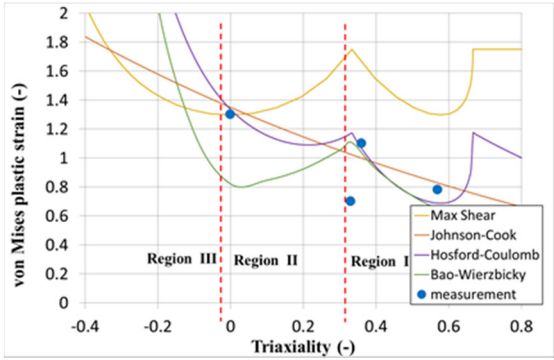Fig. 11 Diagram of shear tests and comparison with numerical simulation

Fig. 12 Graph of fracture curves

Numerical modelling was performed successively with each of the four models. The fracture curves for various triaxiality values are plotted in Fig. 12

Fine blanking experiment

A real-world fine blanking experiment involving a steel washer was carried out in order to validate the material models. The tool used is shown in Fig. 3. The material for fine blanking was laser-cut round specimens of 1.4301 stainless steel of 2 mm thickness.

Four values of tool displacement were used. Three of them led to pre-defined incomplete fine blanking. The fourth specimen was punched out completely. In specimens T1, T2 and T3, the fine blanking operation stopped at displacements 2.1 mm, 3.1 mm and 3.65 mm, respectively; the values include the engagement of the impingement ring. Specimen T4 was blanked completely. Force [kN] vs. displacement [mm] curve was measured, as shown in Fig. 13. The complete fine blanking of the last specimen T4 was simulated because it was most relevant for modelling.

Abaqus/explicit solver was used for FE analysis. An axisymmetric 2D model with controlled displacement was developed. Mesh elements were CAX4R type with a size of 0.05 m. The tools were defined as rigid bodies. The hold-down force of the impingement ring and counterpunch were exerted by springs. The frame of the machine was simulated as a 1D element disposed between the point of application of force and the tool.
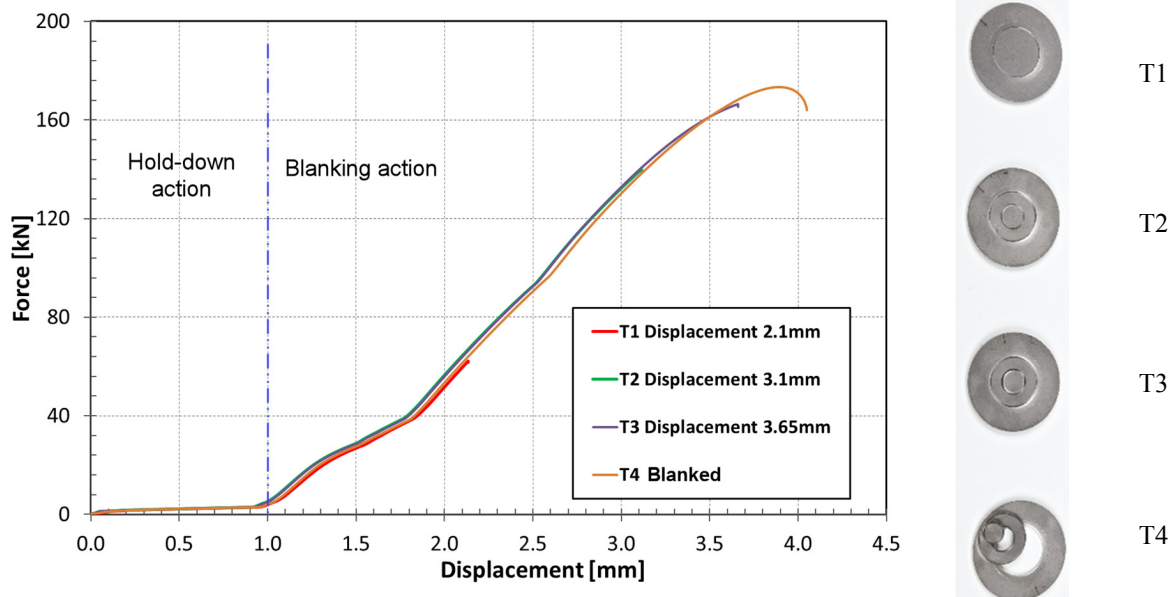

Fig. 13 Force-displacement curves for specimens T1 through T4

Fig. 15 compares measured data and the numerical model. The undefined compliance of the test tool and its parts, such as springs, was simplified in the numerical model, which led to differences between the simulation and the measurement. Although there were small displacement discrepancies, the real-world experiment and the simulation were in a very good overall agreement. The differences between the results of fracture calculations were given by specific model definitions. The dip in the J-C model data is due to damage in compression, where the J-C model reports lower fracture values, whereas the B-W model reports almost infinity.
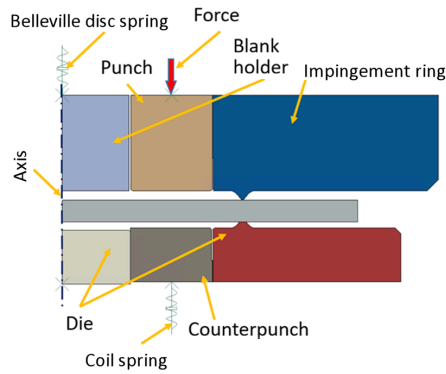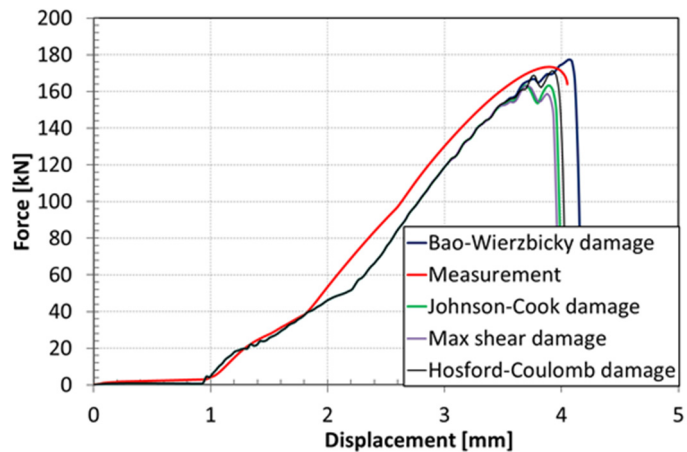
Fig. 14 Fine blanking

Fig. 15 Results of fracture modelling using individual models and comparison with real-world data

Conclusions

In the present paper, a method of finding material constants for Johnson-Cook plasticity and fracture models and Bao-Wierzbicky, Max shear and Hosford-Coulomb fracture models, as well as their validation by means of a technological test is described. Several types of test specimens suitable for calibrating these material models were presented. The models were validated by fine blanking of a precise stainless steel washer. Good agreement was achieved between the measurement and simulations. This means that the calibrated constants offer an accurate description of material behaviour. A material model developed and validated by this procedure is useful in the design and optimization of real-world shearing processes. It was found that the model which was the plainest in terms of calibration data was still fully sufficient for practical engineering use.

Acknowledgement

References

[1] Ł. Bohdal et al., Three Dimensional Finite Element Simulation of Sheet Metal Blanking Process. Applied Mechanics and Materials. 474, 430–435 (2014).

[2] T. Wesner* and P. Hora, Investigation of ductile fracture in fine blanking processes and virtual prediction of scar formation by means of 3d ale simulations, XIII International Conference on Computational Plasticity. Fundamentals and Applications (2015) 562 – 575.

[3] Rund M, Mašek M, Džugan J, Konopík P, Janovec J. Experiment and finite element analysis of U-profile subjected to dynamic loading. Buzaud E, Cosculluela A, Couque H, Cadoni E, eds. EPJ Web of Conferences 2018; 183:2056.

[4] Dalloz, A., Besson, J., Gourgues-Lorenzon, A.F., Sturel, T., and Pineau, A. (2009). Effect of shear cutting on ductility of a dual phase steel. Engineering Fracture Mechanics 76, 1411–1424

[5] Gutknecht, F., Steinbach, F., Hammer, T., Clausmeyer, T., Volk, W., and Tekkaya, A.E. (2016). Analysis of shear cutting of dual phase steel by application of an advanced damage model. Procedia Structural Integrity 2, 1700–1707

[6] Wang, K., and Wierzbicki, T. (2015). Experimental and numerical study on the plane-strain blanking process on an AHSS sheet. International Journal of Fracture 194, 19–36.

[7] Canales, C., Bussetta, P., and Ponthot, J.P. (2017). On the numerical simulation of sheet metal blanking process. International Journal of Material Forming 10, 55–71.

[8] URBÁNEK, Miroslav, TIKAL, Filip. Effective Preparation of Non-linear Material Models by Using Programmed Optimazation Script for Nurimerical Simulation of Sheet Metal Processing. In: Materiali in technologije, 49(2). Ljubljana, 2015. p. 5/291-295. ISSN 1580-2949.

[9] Peirs, J., Verleysen, P., Van Paepegem, W., and Degrieck, J. (2011). Determining the stress-strain behaviour at large strains from high strain rate tensile and shear experiments. International Journal of Impact Engineering 38, 406–415.

[10] Roth, C.C., and Mohr, D. (2018). Determining the strain to fracture for simple shear for a wide range of sheet metals. International Journal of Mechanical Sciences 149, 224–240.

[11] Hosford WF, A generalized isotropic yield criterion. J Appl Mech 1972; 39:607

[12] Wierzbicki, T., Bao, Y., Lee, Y.-W., and Bai, Y. (2005). Calibration and evaluation of seven fracture models. International Journal of Mechanical Sciences 47, 719–743.

[13] SCHMIDT, R.-A., P. HÖFEL, B. REH, F. BIRZER, M. HELLMANN, P. RADEMACHER a H. HOFFMANN. *Cold Forming and Fineblanking: a Handbook on cold processing, steel material properties and part, part design*. 1. Wien: Carl Hanser Verlag GmbH and Company, 2007. ISBN 9783446413504.

[14] Roth, C.C., and Mohr, D. (2016). Ductile fracture experiments with locally proportional loading histories. International Journal of Plasticity 79, 328–354.